ACS OMEGA

http://pubs.acs.org/journal/acsodf

Article

Gecko-Inspired Biomimetic Surfaces with Annular Wedge Structures Fabricated by Ultraprecision Machining and Replica Molding

Tianfeng Zhou, Benshuai Ruan, Jiangtao Che,* Hui Li, Xi Chen, and Zhihong Jiang*

Cite This: *ACS Omega* 2021, 6, 6757−6765

Read Online

ACCESS | Metrics & More | Article Recommendations

ABSTRACT: The current research on gecko-inspired dry adhesives is focused on micropillar arrays with different terminal shapes, such as flat, spherical, mushroom, and spatula tips. The corresponding processing methods are mostly chemical methods, including lithography, etching, and deposition, which not only are complex, expensive, and environmentally unfriendly, but also cannot completely ensure microstructural integrity or performance stability. The present study demonstrates a high-precision, high-efficiency, and green method for the fabrication of a gecko-inspired surface, which can promote its application in dexterous robot hands and mechanical grippers. Based on the bendable lamellar structures of the gecko, annular wedge adhesive surfaces that stick to the finger surfaces of dexterous robot hands to improve their load capacity are proposed and fabricated via a suitable combined processing method of ultraprecision machining and replica molding. The greater the width, the higher the replication integrity, and when the minimum width is 20 μm, the replication error is less than 5.5% due to the superior processing performance of the nickel−phosphorus (Ni−P) plating of the master mold. The fabricated annular wedge structures with an optimized width of 20 μm not only exhibit a strong friction force of up to 35.48 mN under a preload of 20 mN in the GCr15/poly(dimethylsiloxane) (PDMS) friction pair but also demonstrate an obviously improved anisotropic friction characteristic of up to λ = 1.36, as the molecular force exhibits a stronger increase as compared to the decrease of the mechanical force of the structure with a small width.

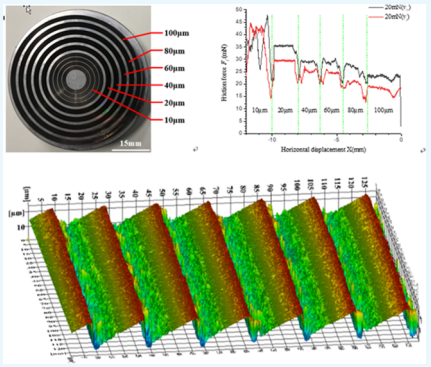

1. INTRODUCTION

With the miniaturization of the hardware structures of dexterous robot hands, the load capacity of the finger is reduced due to the built-in low-power drive motor within a small space, which hinders the promotion and application of the hands. The load capacity can be effectively increased by covering the biomimetic surfaces on the finger surfaces with different microstructures; the characteristics of which primarily determine the adhesion performance.

In nature, geckos exhibit outstanding climbing ability in various environments, especially on smooth glass or ceilings, and therefore, have attracted great interest for biomimetic microstructure research. By the measurement and analysis of the force of a single seta, Autumn et al. found that the strong adhesion of geckos is attributed to the van der Waals force between the thousands of spatulate structures and rough surfaces.[1] Regarding theoretical research, compared to other adhesion mechanisms, such as wet adhesion displayed by tree frogs,[2] mechanical interlocking displayed by snakes,[3] and vacuum suction displayed by octopi,[4] dry adhesion is environment-independent and reusable, and the characteristics of strong attachment and easy detachment provide theoretical support for its application in dexterous robot hands.

It has been observed from scanning electron microscopy (SEM) micrographs of a gecko foot that each toe is composed of thousands of hierarchical structures of cylindrical setae, branches, spatulas, and flat tips of the spatulae.[5] Based on the microstructures of a gecko foot, many gecko-inspired structures have been designed and investigated.[6−11] For instance, the effect of the terminal contact shape on adhesion was systematically studied by Del Campo et al.[12] It was found that the terminal shape plays an important role in determining the adhesive properties and that mushroom and spatulate tips exhibit higher adhesion strength than flat tips, spherical tips, flat tips with rounded edges, and concave tips.[13−17] Moreover, the maximum pull-off force can reach 42 N/cm^2.[18] However, due to its symmetry, the mushroom-like structure cannot achieve rapid adhesion and desorption in different directions, as geckos can. On the contrary, the wedge structure has received increasingly more attention in the research on the anisotropy of gecko-inspired structures due to its asymmetry.[19−22] Three different wall-shaped adhesive microstructures

Received: November 30, 2020
Accepted: February 23, 2021
Published: March 4, 2021

https://dx.doi.org/10.1021/acsomega.0c05804
ACS Omega 2021, 6, 6757−6765

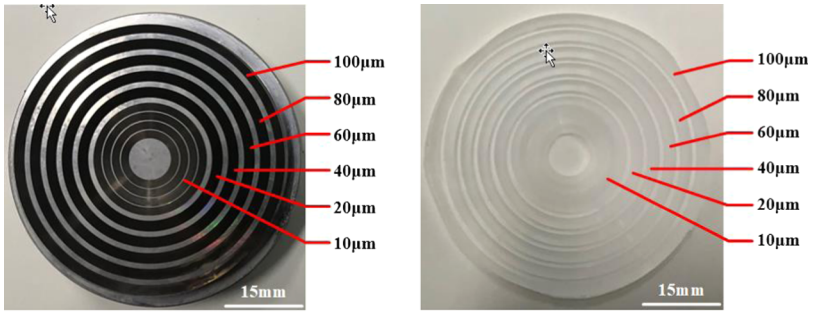

Figure 1. Master mold and PDMS replica of the annular wedge structure.

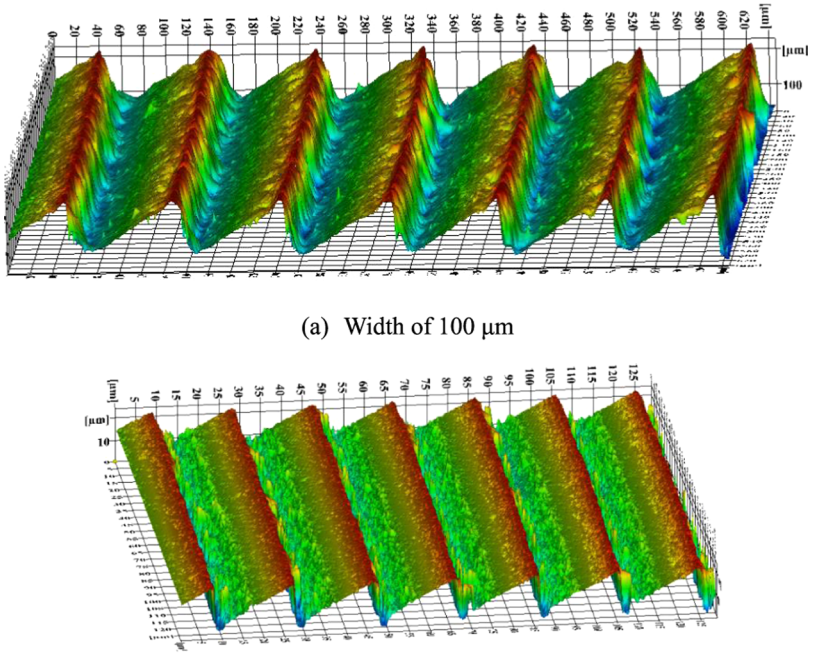

Figure 2. Optical micrographs of microstructures on the master mold with different widths.

inspired by spatula-shaped attachment hairs were designed by Kim et al., and the effects of the pulling angle and preliminary displacement were studied in detail.[23] Kerst et al. fabricated a narrow-angled structure from a metal mold created by sputtering metal and electroplating copper, which did not require a mold release coating and was easy to clean.[24]

According to the feature size of the gecko, biomimetic structures are usually micro/nanostructures. The common techniques for the fabrication of biomimetic structures include lithography, etching, deposition, and self-assembly,[25−30] which could be classified into two types, namely, (1) etching and casting and (2) gas-phase growth. Carbon nanotube fibers have been fabricated by low-pressure chemical vapor deposition (CVD), and the effect of temperature on adhesion has been studied.[31] Moreover, well-defined mushroom-shaped microstructures were fabricated by Wang et al. based on photolithography and molding.[32] Although these methods can produce smaller microstructures, their complex procedures and harsh conditions have hindered their further development. Regarding large-area anisotropic wedge structures, machining technology has attracted great interest due to its high precision and high efficiency.[33−38] Tricinci et al. faithfully reproduced the hierarchical shape of gecko setae via two-photon lithography and studied its effects in terms of its adhesion and friction performances.[39] However, this process is very slow, and large-area preparation is not possible. The method of fabricating wedge molds via ultraprecision diamond cutting was first proposed by Tao et al., and gecko-inspired surfaces were replicated by poly(dimethylsiloxane) (PDMS).[40] However, due to the large amount of heat generated locally in the ultraprecision machining process and the easy deformation of the aluminum mold by pressure or heat, the microstructure precisions of the mold and the PDMS replica were not high. So far, very few research studies have been conducted on the fabrication of biomimetic structures using ultraprecision processing technology, especially in terms of mold machining accuracy and replication error. Moreover, despite the importance of the effects of the width on the real contact area and friction, the friction performance of gecko-inspired wedge structures with different widths remains unknown.

In this research, molds of gecko-inspired annular wedge structures with different widths were first fabricated using ultraprecision diamond cutting on tungsten carbide with a nickel−phosphorus (Ni−P) plating. Then, gecko-inspired

https://dx.doi.org/10.1021/acsomega.0c05804
ACS Omega 2021, 6, 6757−6765

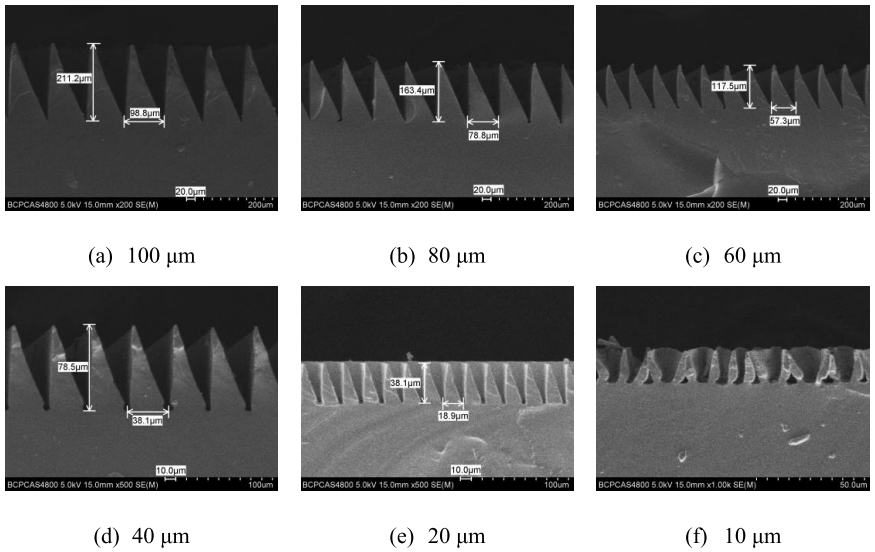

(a) 100 μm (b) 80 μm (c) 60 μm

(d) 40 μm (e) 20 μm (f) 10 μm

Figure 3. SEM micrographs of microstructures of the PDMS replica with different widths.

wedge structures were replicated with PDMS via the tungsten carbide mold. Finally, the effects of different preloads, widths, and angles of the wedge structures and motion directions on the friction property were experimentally investigated with a friction tester in the GCr15/PDMS friction pair. The purpose of this study is to explore the friction mechanism of the gecko cross-scale structure and find the optimal microstructural size to improve the friction force and anisotropy capability, which will provide theoretical support for the widespread use of biomimetic structures in dexterous robot hands and mechanical grippers.

2. RESULTS AND DISCUSSION

2.1. Analysis of Mold Quality. The machining process of the mold of the annular wedge structure was carried out on a Nanoform X Ultra-Precision Machining System (Precitech Corporation), and the fabricated mold is depicted in Figure 1a. The darker part of the mold is the processed wedge structure, while the brighter part is the original Ni−P plating surface, which was polished before machining. The diameter of the mold was 50 mm. Along the radial direction of the mold, from the outside to the inside, the processed microstructure widths were, respectively, 100, 80, 60, 40, 20, and 10 μm. The radial length of the microstructures with widths of 100, 80, 60, 40, and 20 μm was 2 mm. Four groups of 10 μm structures were processed because the structures were too small, and the radial length between them was 1.5 mm.

Before the replica molding process, a preliminary observation of the microstructure of the mold was made using a laser scanning confocal microscope (LEXT OLS5000, Olympus, Japan), and the results are presented in Figure 2. The basic features of the wedge structure, i.e., the vertical surface, the sloping surface, and the sharp corners of the wedge structure, were clearly observed on both the large scale of 100 μm and the small scale of 10 μm. The surface roughness (R_a) values of the sloping surface were 16, 20, 22, 24, 23, and 26 nm, corresponding to the widths of 100, 80, 60, 40, 20, and 10 μm, respectively. The advantages of high precision based on ultraprecision cutting and the high surface quality based on the Ni−P plating were vividly demonstrated.

2.2. Analysis of Replication Integrity. After the replica molding process, the wedge PDMS structure was obtained, as shown in Figure 1b. The width of the biomimetic wedge microstructure is critical to the achievement of high levels of friction and the anisotropy of the annular wedge arrays. Therefore, the accurate control of the structural integrity of the wedge microstructure is necessary for the development of biomimetic surfaces with superior friction performance. Figure 3a−f presents the SEM images of the PDMS replica fabricated with the six widths of 100, 80, 60, 40, 20, and 10 μm, respectively. The integrity of the replicated structure was relatively high between the widths of 100 and 20 μm, whereas the bunching and collapse of the microstructures were evident at 10 μm, as shown in Figure 3f. This phenomenon results from the attraction forces between adjacent low-stiffness wedge microstructures in the demolding process.

The parameters α and w are important factors for the morphological characterization of biomimetic structures. Additionally, w and h can be directly measured from the SEM images, and α can be calculated using $\tan\alpha = w/h$. By analysis and calculation, the accuracy errors of the replicated morphology at different widths were determined, as reported in Figure 4. As the width increased from 20 to 100 μm, the width error ($\Delta(w)$) decreased from 5.5 to 1.2% and the angle error ($\Delta(\tan\alpha)$) decreased from 6.4 to 3.2%; the width error ($\Delta(w)$) and angle error ($\Delta(\tan\alpha)$) are as follows

$$\Delta(w) = \frac{w_{\text{theory}} - w_{\text{experiment}}}{w_{\text{theory}}} \times 100\% \quad (1)$$

$$\Delta(\tan\alpha) = \frac{\tan\alpha_{\text{theory}} - \tan\alpha_{\text{experiment}}}{\tan\alpha_{\text{theory}}} \times 100\% \quad (2)$$

The overall errors of the widths were relatively small, which indicates that the microstructural characteristics of the high-precision mold were well replicated. When the widths were 80 and 100 μm, the replicated structures exhibited particularly high accuracy, which depended on the large gap that could be completely filled by PDMS. The replication accuracy was also maintained at a high level when the widths were 20 and 40 μm, which was due to the high quality of the machine side structure that was conducive to the flow of liquid PDMS. In contrast, at

https://dx.doi.org/10.1021/acsomega.0c05804
ACS Omega 2021, 6, 6757−6765

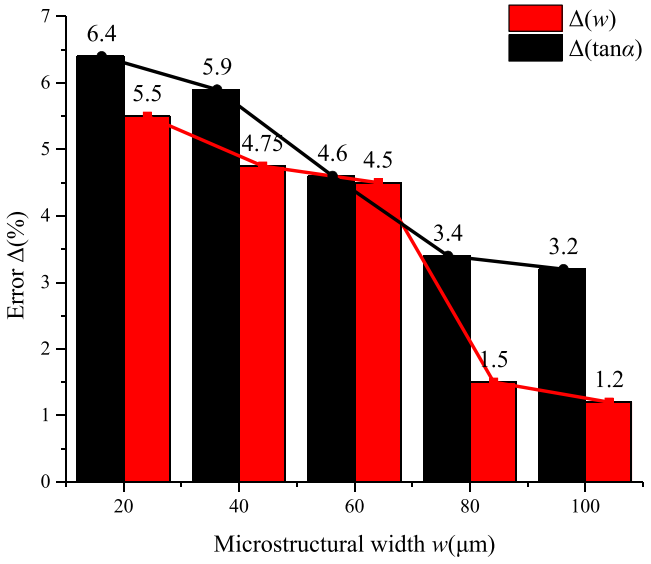

Figure 4. Accuracy errors of the replicated morphology at different widths.

a width of 10 μm, the attraction forces between adjacent low-stiffness wedge microstructures in the demolding process resulted in the collapse of the microstructure and poor replication integrity.

2.3. Analysis of the Friction Property. A UMT TriboLab, Bruker's latest and most advanced mechanical property tester, was used to measure the static and kinetic frictions of the annular wedge structures. In the experiment, a steel ball was aligned with the center of the circular biomimetic structures and then moved in the radial direction to sequentially contact and squeeze the microstructures of different widths.

The influence of the preload on the friction force is shown in Figure 5a. The friction force increased with increasing preload from 5 to 20 mN. The increase of the preload made the microstructures bend and deform more fully, thereby increasing the real contact areas. Besides, the obvious stick–slip phenomena can be observed, as shown in Figure 5b. In the initial stage of friction, the ball and the microstructure were relatively static, and the friction force increased with the increase of time. When the relative sliding emerged, the friction changed from static friction to kinetic friction and the force decreased due to the damage of the contact surfaces. The preload affected not only the maximum friction force but also the first stick–slip distance. As shown in Figure 5a, the first stick–slip distance increased as the preload increased. It can be explained that the larger elastic deformation energy was generated by the larger preload, which accumulated in the microstructure.

The influence of the biomimetic structure width on the friction force is shown in Figure 6. Under the same preload, the friction force increased as the width decreased because a smaller width led to the higher density of the wedge structures. The real contact area was related not only to the size but also to the density of the microstructure. However, the friction of the biomimetic structures with a width of 10 μm was much higher than those of the structures with other widths. This is

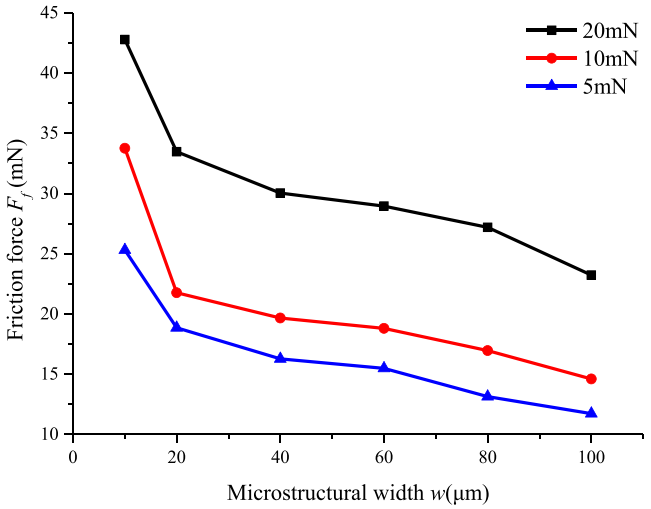

Figure 6. Influence of the width of biomimetic structures on the friction force of the sample under different preloads.

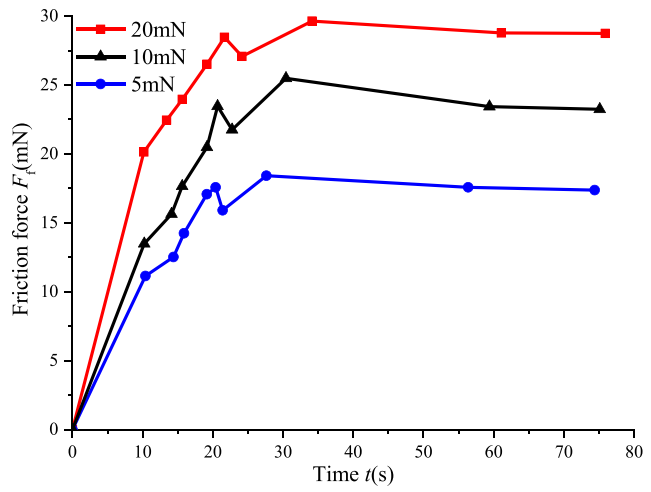

(a) Friction force-time curve

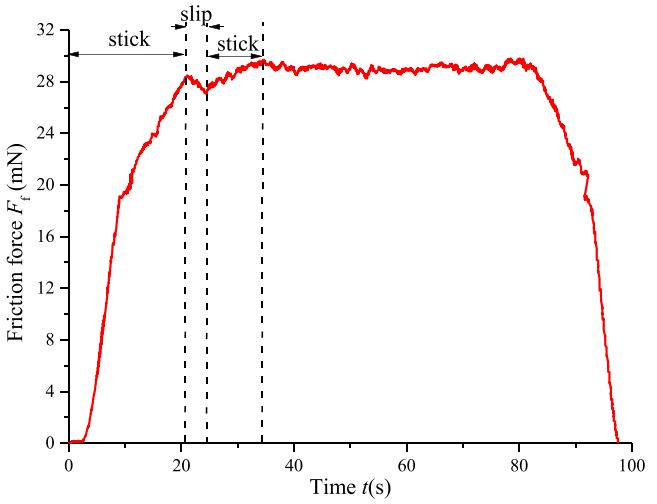

(b) Stick-slip phenomenon(20mN)

Figure 5. Influence of shearing time on the friction force of the sample under different preloads (sample with a 40 μm wedge structure).

https://dx.doi.org/10.1021/acsomega.0c05804
ACS Omega 2021, 6, 6757–6765

due to the bunching and collapse of the biomimetic structure, which is consistent with the experimental phenomenon, as shown in Figure 3f.

The angle of the microwedge also had an important influence on the friction force. Under the same preload, at a width of the microstructure of 40 μm, the friction force decreased as the angle of the microwedge increased, as illustrated in Figure 7. When the width of the microstructure

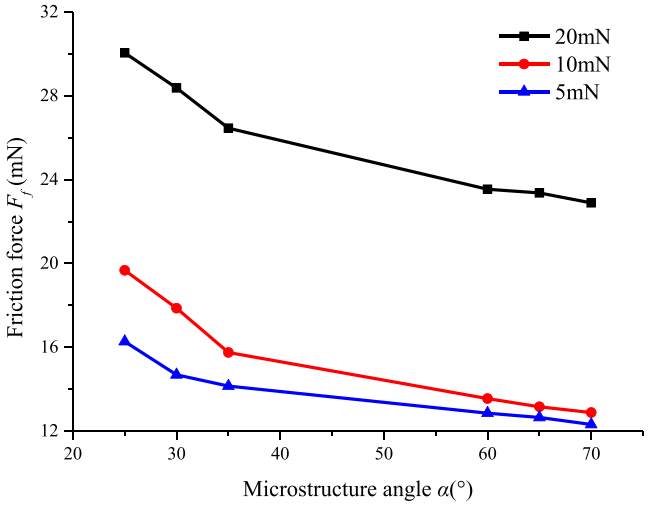

Figure 7. Influence of the angle of biomimetic structures on the friction force of the sample under different preloads.

was constant, increasing the angle reduced the height of the microstructure and made it difficult to be deformed. The influence of the angle on the friction force gradually weakened as the angle increased.

Regardless of whether the preload was 20, 10, or 5 mN, with the change of the widths of the biomimetic structures from 100 to 10 μm, the friction force exhibited the same increasing trend, which corresponds to the two parts of the binomial theorem of tribology

$$F = \alpha A + \beta W \quad (3)$$

where A is the real contact area, W is the normal force, and α and β are the friction coefficients determined by the physical and mechanical properties of the friction surface, respectively.[34] According to the binomial theorem of tribology, friction is composed of the mechanical force caused by overcoming mechanical engagement and the molecular force caused by resisting molecular attraction. When the width decreased from 100 to 20 μm, the mechanical force and the molecular force were in competition during the entire process. For a large-scale width of 100 μm, due to the high rigidity of the microstructure, it did not easily bend and deform after compression, which resulted in a small side contact area. At this time, the friction force was mainly determined by the mechanical force. With the reduction of the width, the structure was more susceptible to deformation under the preload, and the contact area of the side surface increased. When the width of the microstructure decreases from 100 to 20 μm, the effect of the mechanical force also decreases, while the effect of the molecular force increases. With the decrease of the width to 20 μm, the real side contact area further increased due to the increase of the number of microstructures per unit area and the more complete compression deformation. At this time, the friction force was mainly determined by the molecular force, which corresponds to the real structure of the gecko. The excellent friction property of the gecko is determined by its hierarchical structure across scales, including the mesoscale lamellae, microscale setae, and nanoscale spatulae. It is the multiscale interaction that endows the gecko with excellent climbing performance.

The influence of the anisotropy of biomimetic structures on the friction force is shown in Figure 8. Figure 8a reveals that the stable friction of the microstructure with a width of 20 μm reached 22.72 mN under a preload of 10 mN and further increased to 35.48 mN under a preload of 20 mN in the gripping direction. The increase of the preload caused the microstructures to bend and deform more fully, thereby increasing the real contact areas. Additionally, as shown in Figure 8b, under the same preload, the friction coefficient

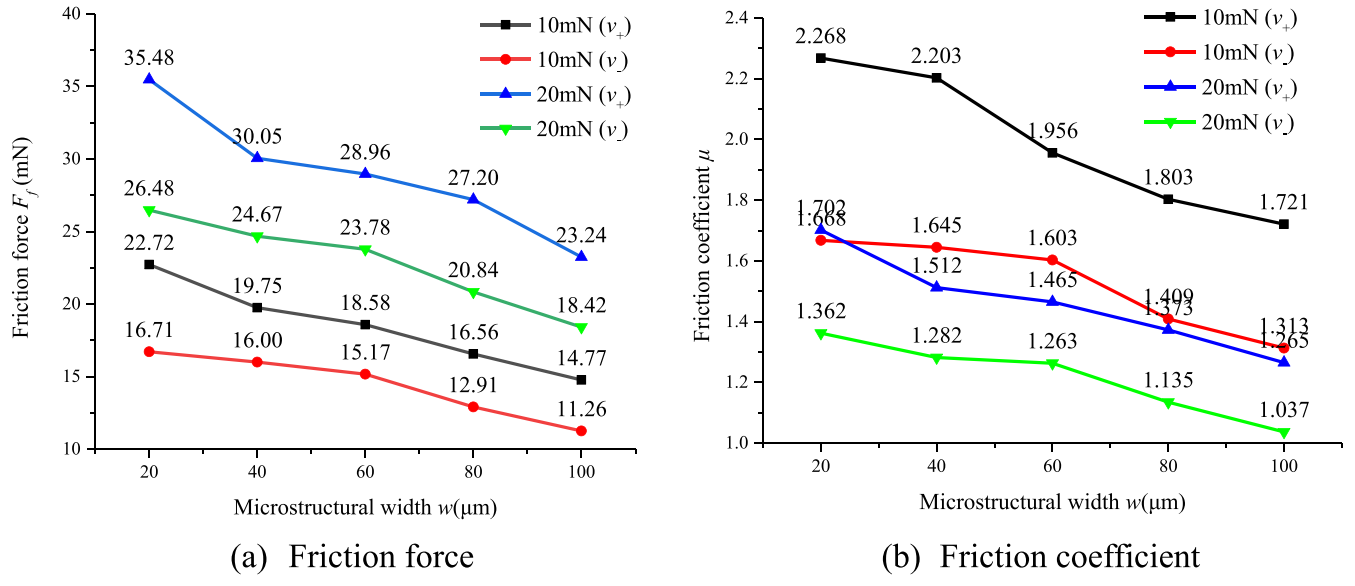

Figure 8. Friction properties of biomimetic structures under different preloads.

https://dx.doi.org/10.1021/acsomega.0c05804
ACS Omega 2021, 6, 6757−6765

increased with the decrease in the width, which is similar to the trend of the friction force. Compared with the other microstructures with widths from 100 to 40 μm, the microstructure with a width of 20 μm exhibited the greatest friction force due to the largest side contact area and the largest friction coefficient.

Although both $F_f(v_+)$ and $F_f(v_-)$ increased with the decrease of the width, the magnitude of the increase was not the same. To evaluate the anisotropic friction characteristics of the gecko-inspired microstructures, the parameter λ, which is the ratio of the friction coefficient at v_+ to that at v_-, is introduced as follows[41]

$$\lambda = \frac{\mu(v_+)}{\mu(v_-)} \quad (4)$$

Figure 9 exhibits the anisotropic properties of the gecko-inspired arrays with different widths under the preloads of 10 and 20 mN. The value of $F_f(v_-)$ increased slowly and more evenly due to the more uniform deformation of the vertical surface of the wedge structure, while the value of $F_f(v_+)$ increased quickly due to the side contact area of the sloping surface of the wedge structure. The real side contact area increased slowly at the large width scale due to the small deformation when the structure was compressed, whereas it increased quickly at the small width scale because the microstructure had been completely deformed and the number of microstructures per unit area increased. Therefore, the anisotropic properties decreased at first and then increased with the decrease of the width. There would be a minimum point at which the mechanical force would be reduced to a relatively small value and the molecular force would be about to increase substantially.

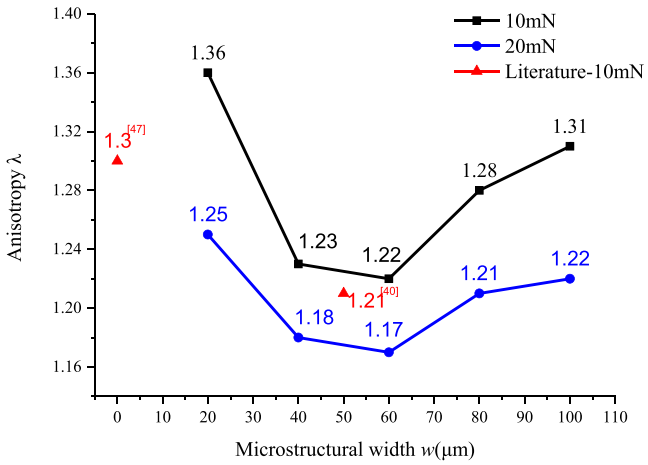

Figure 9. Anisotropic properties of biomimetic structures under different widths.

According to the curve trend of the 10 test points under different preloads shown in Figure 9, combined with the fact that the molecular force started to work gradually when the width was small, it is conjectured that there will be a minimum value between the widths of 40 and 60 μm. Compared to a microstructure with λ (w = 50 μm) = 1.21 under a preload of 10 mN, as reported in a previous study,[40] the values of the parameter λ for all of the microstructures with widths from 20 to 100 μm were larger than the reported value, and λ (w = 50 μm) is exactly located between λ (w = 40 μm) and λ (w = 60 μm), which verifies the conjecture of the minimum value based on the binomial theorem of tribology. Compared with a nanostructure with λ =1.30 under a preload of 10 mN reported in another previous study,[41] the microstructure with λ (w = 20 μm) = 1.36 exhibited a better anisotropic property. This is because the fabricated nanostructures easily collapsed and bunched, which affected the friction performance. It is very similar to the friction characteristics exhibited by the biomimetic structure with a width of 10 μm. The friction anisotropy can be further improved by optimizing the biomimetic structural parameters, increasing preloads, and considering the influence of the tilt angle.

3. CONCLUSIONS

In this research, a biomimetic structure was designed and fabricated, and its friction properties were studied. The conclusions of this work can be drawn as follows:

(1) Annular wedge adhesive surfaces that mimic the bendable lamellar structures of geckos were designed and fabricated by a combined ultraprecision machining and replica molding processing method.

(2) An optimum width of 20 μm of the gecko-inspired annular wedge structure based on the fabricated Ni−P plating master mold was found to achieve high integrity and precision without damage. Additionally, at this size, the structure exhibited strong friction force and obvious anisotropic characteristics in the GCr15/PDMS friction pair.

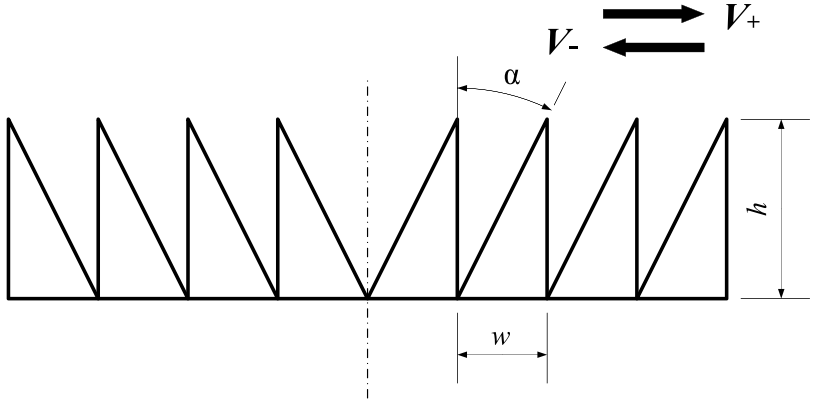

Figure 10. Schematic diagram of the biomimetic structure.

https://dx.doi.org/10.1021/acsomega.0c05804
ACS Omega 2021, 6, 6757−6765

(3) The friction force is composed of mechanical force and molecular force, which are constantly in competition. For the cross-scale hierarchical structure derived from gecko feet, mechanical forces play a dominant role in the macrostructure, while molecular forces play a leading role in the microstructure, and there is a minimum value of friction anisotropy between the widths of 40 and 60 μm.

The annular wedge structure developed in this study has strong friction force and obvious anisotropy and can realize the high-precision, high-efficiency, and green fabrication of a gecko-inspired surface, which can promote its application in dexterous robot hands and mechanical grippers.

4. EXPERIMENTAL SECTION

4.1. Design of Gecko-Inspired Annular Wedge Structures. The skin on the toes of a gecko comprises a complex hierarchical structure of mesoscale lamellae, microscale setae, and nanoscale spatulae.[5] The lamellae located on the toes are 1−2 mm in length and are covered in microscale setae with a length of 30−130 μm. The excellent climbing performance of the gecko is due to the hierarchical structure (lamellae−setae−spatulae) that enables a large real contact area between the gecko skin and the mating surface.

Inspired by the bendable lamellar structure of the gecko,[42] an annular wedge structure was designed, as shown in Figure 10. Compared with the micropillar array, the annular structure can effectively avoid lateral collapse and root fracture due to the complete bottom connection in the circumferential direction and is also suitable for large-area fabrication via the ultraprecision machining method. In addition, the wedge structure that mimics the bendable lamellae of the gecko is asymmetric, which provides anisotropic tribological properties depending upon the direction in which the adhesive surface is sheared. The wedge structures were constructed with different widths to generate the friction property upon shearing by changing the real contact area.

4.2. Fabrication of the Ni−P Plating Master Mold. Although aluminum is the most commonly used mold material, it is susceptible to thermal deformation during ultraprecision cutting, which affects the machining accuracy.[43] In the present study, tungsten carbide with a Ni−P plating with a thickness of 600 μm was used as the mold material. Compared with tungsten carbide materials, the Ni−P plating can not only reduce the hardness of the mold materials, which can reduce tool wear and improve the service life of the materials, but also enhance the quality of the machined surface due to its superior uniformity, smoothness, and compactness.[44]

According to the wedge structure illustrated in Figure 10, the parameter α represents the angle between the vertical surface and the sloping surface of the wedge structure, which is determined by the knifepoint angle of the diamond tool. The parameter w represents the width of a single biomimetic structure, as well as the interval between the biomimetic structures. The parameter h represents the height, i.e., the depth, of a single biomimetic structure. According to the length of the setae, which is 30−130 μm, the width of the biomimetic structure of a signal seta w = 14−61 μm is calculated using the equation $w = \tan\alpha \times h$. Therefore, the widths selected for the experiment were respectively 10, 20, 40, 60, 80, and 100 μm, and the geometric parameters of the diamond tool and the cutting parameters are reported in Table 1.

Table 1. Experimental Conditions of Annular Wedge Structures Machined by Diamond Cutting

cutting speed v (mm/min)	370
feed rate (mm/rev)	1
microstructure width w (μm)	10, 20, 40, 60, 80, 100
microstructure angle α (deg)	25, 30, 35, 60, 65, 70
tool material	diamond
rake angle (deg)	0
clearance angle (deg)	15
corner radius (μm)	5
knifepoint angle of the diamond tool (deg)	25, 60

The friction properties of biomimetic structures are mainly determined by the contact area.[45] The relationship between the real contact area and the widths of the biomimetic structure can be verified in the finite element software ABAQUS. In the finite element method (FEM) simulation, PDMS is an organic polymer with elastic solid and viscoelastic material characteristics, so the cohesive zone mode (CZM) is used in the simulation, and the important parameters including CZM parameters, material parameters, and motion parameters are listed in Table 2.[46−48] The two-dimensional (2D) simulation results are shown in Figure 11. As the width decreased from 100 to 20 μm, the real contact length increased from 6.722 to 9.898 μm. Therefore, increasing the real contact area can be achieved by processing more microstructures per unit area.

Table 2. Important Parameters in the FEM Simulation

part	parameters	values
cohesive zone model	maximum cohesive traction T_{max}	0.0154 MPa
	initial critical stiffness K_0	0.07689 N/mm^3
	cohesive fracture energy G_c	0.00198 J/mm^2
material	Young's modulus E	1.8 MPa
	Poisson's ratio μ	0.48
	viscosity coefficient η	1×10^{-15}
motion	preload F	10 mN
	sliding speed v	0.02 mm /s
	shearing distance l	2 mm

4.3. Fabrication of PDMS Annular Wedge Arrays. PDMS is widely used as a gecko-inspired fiber array material due to its advantages of easy curing, low Young's modulus, low surface energy, low cost, and chemical stability.[49] For this research, SYLGARD 184 was purchased from Dow Silicones Corporation and was used as the sample base. The replica molding process can be roughly divided into three subprocesses.[50] (1) The basic component (SYLGARD 184A) was mixed with a curing agent (SYLGARD184B) at a mass ratio of 10:1. After even mixing, it was vacuumed until all bubbles disappeared. (2) The liquid PDMS was carefully poured onto the fabricated Ni−P plating master mold of the annular wedge arrays with varying geometries and cured at 70 °C for 2 h. (3) The master mold covered with PDMS was then taken out and cooled to room temperature. Subsequently, the PDMS replicas were carefully removed from the master mold in one direction.

https://dx.doi.org/10.1021/acsomega.0c05804
ACS Omega 2021, 6, 6757−6765

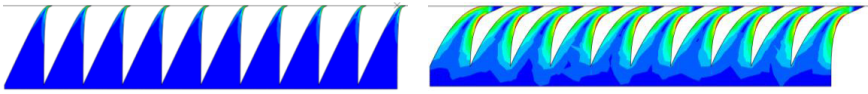

(a) width of 100 μm (b) width of 20 μm

Figure 11. 2D simulations of deformation of microstructures with different widths.

4.4. Friction Measurements. The macroscopic friction of the annular wedge arrays was evaluated using a UMT (Universal Mechanical Tester) TriboLab (Bruker, Germany) at a relative humidity of 45% and an ambient temperature of 25 °C. A circular PDMS replica was attached to a steel ball with a diameter of 2 mm as the friction pair under controlled preloads of 5, 10, and 20 mN, respectively, and slipped at a speed of 0.02 mm/s using a motorized stage. The stroke and frequency of 20 Hz-@25 mm in the reciprocating motion module were selected. For statistical significance, friction force measurement was conducted five times for different directions under identical conditions.

AUTHOR INFORMATION

Corresponding Authors

Jiangtao Che − *School of Mechatronic Engineering, Beijing Institute of Technology, Beijing 100081, P. R. China*; orcid.org/0000-0002-5456-1538; Email: cjtsyq@163.com

Zhihong Jiang − *School of Mechatronic Engineering, Beijing Institute of Technology, Beijing 100081, P. R. China*; Email: jiangzhihong@bit.edu.cn

Authors

Tianfeng Zhou − *School of Mechanical Engineering, Beijing Institute of Technology, Beijing 100081, P. R. China*

Benshuai Ruan − *School of Mechanical Engineering, Beijing Institute of Technology, Beijing 100081, P. R. China*

Hui Li − *School of Mechatronic Engineering, Beijing Institute of Technology, Beijing 100081, P. R. China*

Xi Chen − *School of Mechatronic Engineering, Beijing Institute of Technology, Beijing 100081, P. R. China*

Complete contact information is available at: https://pubs.acs.org/10.1021/acsomega.0c05804

Author Contributions

The paper was written with the contributions of all authors. All authors have given approval to the final version of the paper.

Notes

The authors declare no competing financial interest.

ACKNOWLEDGMENTS

This work was supported in part by the National Key Research and Development Program of China under Grant No. 2018YFB1305300 and the National Natural Science Foundation of China under Grant Nos. 61733001, 61873039, U1913211, and U1713215.

REFERENCES

(1) Autumn, K.; Liang, Y. A.; Hsieh, S. T.; Zesch, W.; Chan, W. P.; Kenny, T. W.; Fearing, R.; Full, R. J. Adhesive Force of a Single Gecko Foot-Hair. *Nature* **2000**, *405*, 681−685.

(2) Drotlef, D. M.; Stepien, L.; Kappl, M.; Barnes, W. P.; Butt, H. J.; Campo, A. Insights into the Adhesive Mechanisms of Tree Frogs Using Artificial Mimics. *Adv. Funct. Mater.* **2013**, *23*, 1137−1146.

(3) Filippov, A. E.; Gorb, S. N. Modelling of the Frictional Behaviour of the Snake Skin Covered by Anisotropic Surface Nanostructures. *Sci. Rep.* **2016**, *6*, No. 23539.

(4) Baik, S.; Kim, D. W.; Park, Y.; Lee, T. J.; Bhang, S. H.; Pang, C. A Wet-Tolerant Adhesive Patch Inspired by Protuberances in Suction Cups of Octopi. *Nature* **2017**, *546*, 396−400.

(5) Bhushan, B. Adhesion of Multi-Level Hierarchical Attachment Systems in Gecko Feet. *J. Adhes. Sci. Technol.* **2007**, *21*, 1213−1258.

(6) Arzt, E.; Gorb, S.; Spolenak, R. From Micro to Nano Contacts in Biological Attachment Devices. *Proc. Natl. Acad. Sci. U.S.A.* **2003**, *100*, 10603−10606.

(7) Kim, S.; Sitti, M. Biologically Inspired Polymer Microfibers with Spatulate Tips as Repeatable Fibrillar Adhesives. *Appl. Phys. Lett.* **2006**, *89*, No. 261911.

(8) Gorb, S. N.; Varenberg, M. Mushroom-Shaped Geometry of Contact Elements in Biological Adhesive Systems. *J. Adhes. Sci. Technol.* **2007**, *21*, 1175−1183.

(9) Wang, Y.; Tian, H. M.; Shao, J. Y.; Sameoto, D.; Li, X. M.; Wang, L.; Hu, H.; Ding, Y. C.; Lu, B. H. Switchable Dry Adhesion with Step-Like Micropillars and Controllable Interfacial Contact. *ACS Appl. Mater. Interfaces* **2016**, *8*, 10029−10037.

(10) Tan, D.; Wang, X.; Liu, Q.; Shi, K.; Yang, B.; Liu, S.; Wu, Z. S.; Xue, L. Switchable Adhesion of Micropillar Adhesive on Rough Surfaces. *Small* **2019**, *15*, No. 1904248.

(11) Croll, A. B.; Hosseini, N.; Bartlett, M. D. Switchable Adhesives for Multifunctional Interfaces. *Adv. Mater. Technol.* **2019**, *4*, No. 1900193.

(12) Del Campo, A.; Greiner, C.; Arzt, E. Contact Shape Controls Adhesion of Bioinspired Fibrillar Surfaces. *Langmuir* **2007**, *23*, 10235−10243.

(13) Gorb, S.; Varenberg, M.; Peressadko, A.; Tuma, J. Biomimetic Mushroom-Shaped Fibrillar Adhesive Microstructure. *J. R. Soc., Interface* **2007**, *4*, 271−275.

(14) Murphy, M. P.; Aksak, B.; Sitti, M. Gecko-Inspired Directional and Controllable Adhesion. *Small* **2009**, *5*, 170−175.

(15) Sameoto, D.; Sharif, H.; Menon, C. Investigation of Low Pressure Adhesion Performance of Mushroom Shaped Biomimetic Dry Adhesives. *J. Adhes. Sci. Technol.* **2012**, *26*, 2641−2652.

(16) Seo, S.; Lee, J.; Kim, K. S.; Ko, K. H.; Lee, J. H.; Lee, J. Anisotropic Adhesion of Micropillars with Spatula Pads. *ACS Appl. Mater. Interfaces* **2014**, *6*, 1345−1350.

(17) Varenberg, M.; Pugno, N. M.; Gorb, S. N. Spatulate Structures in Biological Fibrillar Adhesion. *Soft Matter* **2010**, *6*, 3269−3272.

(18) Sameoto, D.; Sharif, H.; Menon, C. Investigation of Low Pressure Adhesion Performance of Mushroom Shaped Biomimetic Dry Adhesives. *J. Adhes. Sci. Technol.* **2012**, *26*, 2641−2652.

(19) Parness, A.; Soto, D.; Esparza, N.; Gravish, N.; Wilkinson, M.; Autumn, K.; Cutkosky, M. A Microfabricated Wedge-Shaped Adhesive Array Displaying Gecko-Like Dynamic Adhesion, Directionality and Long Lifetime. *J. R. Soc., Interface* **2009**, *6*, 1223−1232.

(20) Day, P.; Eason, E. V.; Esparza, N.; Christensen, D.; Cutkosky, M. Microwedge Machining for the Manufacture of Directional Dry Adhesives. *J. Micro Nano-Manuf.* **2013**, *1*, No. 011001.

(21) Alizadehyazdi, V.; Simaite, A.; Spenko, M. Evaluation of Material Properties for Practical Microstructured Adhesives: Low Dust Adhesion and High Shear Strength. *ACS Appl. Mater. Interfaces* **2019**, *11*, 8654−8666.

(22) Kasem, H.; Tsipenyuk, A.; Varenberg, M. Biomimetic Wall Shaped Hierarchical Microstructure for Gecko-Like Attachment. *Soft Matter* **2015**, *11*, 2909−2915.

(23) Kim, J. K.; Varenberg, M. Biomimetic Wall-Shaped Adhesive Microstructure for Shear-Induced Attachment: The Effects of Pulling Angle and Preliminary Displacement. *J. R. Soc., Interface* **2017**, *14*, No. 20170832.
(24) Kerst, C.; Suresh, S. A.; Cutkosky, M. R. Creating Metal Molds for Directional Gecko-Inspired Adhesives. *J. Micro Nano-Manuf.* **2020**, *8*, No. 011004.
(25) Yi, H.; Kang, M.; Kwak, M. K.; Jeong, H. E. Simple and Reliable Fabrication of Bioinspired Mushroom-Shaped Micropillars with Precisely Controlled Tip Geometries. *ACS Appl. Mater. Interfaces* **2016**, *8*, 22671−22678.
(26) Song, J.; Mengüc, Y.; Sitti, M. Enhanced Fabrication and Characterization of Gecko-Inspired Mushroom-Tipped Microfiber Adhesives. *J. Adhes. Sci. Technol.* **2013**, *27*, 1921−1932.
(27) Chary, S.; Tamelier, J.; Turner, K. A Microfabricated Gecko Inspired Controllable and Reusable Dry Adhesive. *Smart Mater. Struct.* **2013**, *22*, No. 025013.
(28) Jo, W.; Choi, J.; Kang, H. S.; Kim, M.; Baik, S.; Lee, B. J.; Pang, C.; Kim, H. T. Programmable Fabrication of Submicrometer Bent Pillar Structures Enabled by a Photoreconfigurable Azopolymer. *ACS Appl. Mater. Interfaces* **2020**, *12*, 5058−5064.
(29) Brinksmeier, E.; Karpuschewski, B.; Yan, J. W.; Schonemann, L. Manufacturing of Multiscale Structured Surfaces. *CIRP Ann.* **2020**, *69*, 717−739.
(30) Malshe, A. P.; Bapat, S.; Rajurkar, K. P.; Haitjema, H. Bio-Inspired Textures for Functional Applications. *CIRP Ann.* **2018**, *67*, 627−650.
(31) Xu, M.; Du, F.; Ganguli, S.; Roy, A.; Dai, L. M. Carbon Nanotube Dry Adhesives with Temperature-Enhanced Adhesion Over a Large Temperature Rang. *Nat. Commun.* **2016**, *7*, No. 13450.
(32) Wang, Y.; Hu, H.; Shao, J. Y.; Ding, Y. C. Fabrication of Well-Defined Mushroom-Shaped Structures for Biomimetic Dry Adhesive by Conventional Photolithography and Molding. *ACS Appl. Mater. Interfaces* **2014**, *6*, 2213−2218.
(33) Yang, Y.; Guo, P. Global Tool Path Optimization of High-Resolution Image Reproduction in Ultrasonic Modulation Cutting for Structural Coloration. *Int. J. Mach. Tools Manuf.* **2019**, *138*, 14−26.
(34) Brinksmeier, E.; Karpuschewski, B.; Yan, J. W.; Schonemann, L. Manufacturing of Multiscale Structured Surfaces. *CIRP Ann.* **2020**, *69*, 717−739.
(35) Zhou, T. F.; Xu, R. Z.; Ruan, B. S.; He, Y. P.; Liang, Z. Q.; Wang, X. B. Study on New Method and Mechanism of Microcutting-Etching of Microlens Array on 6H-SiC Mold by Combining Single Point Diamond Turning with Ion Beam Etching. *J. Mater. Process. Technol.* **2020**, *278*, No. 116510.
(36) Feng, G.; Sagapuram, D. Size Effect and Friction in Cutting of Metals on the Small Scale. *CIRP Ann.* **2020**, *69*, 77−80.
(37) Lee, Y. J.; Wang, H. Current Understanding of Surface Effects in Microcutting. *Mater. Des.* **2020**, *192*, No. 108688.
(38) He, Y. P.; Zhou, T. F.; Dong, X. B.; Liu, P.; Zhao, W. X.; Wang, X. B.; Hu, Y.; Yan, J. W. Generation of High-Saturation Two-Level Iridescent Structures by Vibration-Assisted Fly Cutting. *Mater. Des.* **2020**, *193*, No. 108839.
(39) Tricinci, O.; Eason, E. V.; Filippeschi, C.; Mondini, A.; Mazzolai, B.; Pugno, N. M.; Cutkosky, M. R.; Greco, F.; Mattoli, V. Approximating Gecko Setae Via Direct Laser Lithography. *Smart Mater. Struct.* **2018**, *27*, No. 075009.
(40) Tao, D. S.; Gao, X.; Lu, H. Y.; Liu, Z. Y.; Li, Y.; Tong, H.; Pesika, N.; Meng, Y. G.; Tian, Y. Controllable Anisotropic Dry Adhesion in Vacuum: Gecko Inspired Wedged Surface Fabricated with Ultraprecision Diamond Cutting. *Adv. Funct. Mater.* **2017**, *27*, No. 1606576.
(41) Zhou, M.; Liu, K.; Wan, J.; li, X.; Jiang, K. L.; Zeng, H. B.; Zhang, X. J.; Meng, Y. G.; Wen, S. Z.; Zhu, H. W.; Tian, Y. Anisotropic Interfacial Friction of Inclined Multiwall Carbon Nanotube Array Surface. *Carbon* **2012**, *50*, 5372−5379.
(42) Hu, H.; Tian, H. M.; Shao, J. Y.; Li, X. M.; Wang, Y.; Wang, Y.; Tian, Y.; Lu, B. H. Discretely Supported Dry Adhesive Film Inspired by Biological Bending Behavior for Enhanced Performance on a Rough Surface. *ACS Appl. Mater. Interfaces* **2017**, *9*, 7752−7760.
(43) Brinksmeier, E.; Karpuschewski, B.; Yan, J. W.; Schonemann, L. Manufacturing of Multiscale Structured Surfaces. *CIRP Ann.* **2020**, *69*, 717−739.
(44) Zhou, T. F.; He, Y. P.; Yu, Q.; Liang, Z. Q.; Li, S. D.; Liu, X. H.; Dong, X. B.; Wang, X. B. Study on Electroless Composite Plating for an Ni- P Bond Micro Diamond Wheel. *J. Mater. Process. Technol.* **2020**, *279*, No. 116561.
(45) Li, X. S.; Tao, D. S.; Lu, H. Y.; Bai, P. P.; Liu, Z. Y.; Ma, L. R.; Meng, Y. G.; Tian, Y. Recent Developments in Gecko-Inspired Dry Adhesive Surfaces from Fabrication to Application. *Surf. Topogr.: Metrol. Prop.* **2019**, *7*, No. 023001.
(46) Zhang, Z. J.; Paulino, G. H. Cohesive Zone Modeling of Dynamic Failure in Homogeneous and Functionally Graded Materials. *Int. J. Plast.* **2005**, *21*, 1195−1254.
(47) Wu, X. Q.; Lian, Q.; Li, D. C.; Jin, Z. M. Tilting Separation Analysis of Bottom-up Mask Projection Stereolithography Based on Cohesive Zone Model. *J. Mater. Process. Technol.* **2017**, *243*, 184−196.
(48) Kern, M. D.; Long, R.; Rentschler, M. E. A Representative Volume Element Model for the Adhesion Between a Micro-Pillared Surface and a Compliant Substrate. *Mech. Mater.* **2018**, *119*, 65−73.
(49) Qi, D. P.; Zhang, K. Y.; Tian, G. W.; Jiang, B.; Huang, Y. D. Stretchable Electronics Based on PDMS Substrates. *Adv. Mater.* **2021**, No. 2003155.
(50) Liu, M.; Peng, Z. L.; Yao, Y.; Yang, Y. Z.; Chen, S. H. Flexible Functional Surface for Efficient Water Collection. *ACS Appl. Mater. Interfaces* **2020**, *12*, 12256−12263.

https://dx.doi.org/10.1021/acsomega.0c05804
ACS Omega 2021, 6, 6757−6765